2 Insulator, Metal, or Superconductor: The Criteria

Richard T. Scalettar
University of California
Physics Department, Davis CA 95616

Contents

1 Introduction

In the United States (and perhaps also around the world) we have a joke about some students' tendency to try to understand physics by memorizing equations: In comprehending electric circuits, we say, it is important that such students completely master Ohm's three laws for current flow in a metal,

$$V = IR \qquad\qquad I = V/R \qquad\qquad R = V/I \ . \qquad\qquad (1)$$

In this chapter, we shall present the subtle relations between resistance, voltage and current, and come to grips with the equations and the deep concepts governing metallic and insulating behavior, and their extension to superconductors. We will see that there is considerably more depth to the field than Ohm's Three Laws, as represented by Eq. (1).

The difference between metals, insulators, and superconductors can be precisely defined, and illustrated, within the framework of tight-binding Hamiltonians (TBH). That will be our primary language here. In addition to developing some analytic approaches to the solution of these Hamiltonians, and hence their characterization into distinct charge transport categories, a good fraction of the material will involve a discussion of how to implement the concepts and equations in precise calculational frameworks, including exact diagonalization and Quantum Monte Carlo (QMC).

The organization of this chapter is as follows. We first describe, in a rather qualitative way, the different types of insulators (band, Anderson, and Mott) which can arise. Our criteria for insulating behavior will focus on the appearance of a gap in the single particle energy levels (band insulator), the appearance of localized eigenfunctions in the presence of disorder (Anderson insulator), or the possibility that interactions between electrons are so strong that motion of electrons is inhibited (Mott insulator). The first two cases can be addressed with some precision with simple calculations, but the latter is much more challenging. In fact, it is fair to say that a full understanding of Mott insulating behavior has not yet been achieved, an especially unfortunate state of affairs since out of Mott insulators many of the most interesting new materials and novel physics develops.

The second part of the chapter develops a more formal set of mathematical criteria for distinguishing metals, insulators, and superconductors, one which focussed directly on the current-current correlation function (and hence, in a sense, can be viewed as a proper treatment of the quantities in Eq. (1)!) This closely follows the discussion of Scalapino, White, and Zhang in Ref. [1]. These criteria will be shown to give sensible results both in simple analytic treatments and also with QMC methods. In the latter case, disorder can also be included, along with interactions.

The final section will outline alternative approaches to distinguishing metallic, insulating, and superconducting behavior which involve an approximate formula for the conductivity and an examination of the single particle spectral function.

2 A brief introduction to tight-binding Hamiltonians Metals and band insulators

Tight-Binding Hamiltonians (TBH) allow for a simplified description of electrons in a solid, which complements methods like density functional theory. Rather than calculate the wave functions in continuum space, one instead focuses on a collection of discrete sites or orbitals which the electrons can occupy and, between which, make transitions. We will assume the student has some familiarity with second quantization, which forms the language of TBHs. We begin with the simplest TBH

$$\hat{H} = -t \sum_{\langle \mathbf{j,l} \rangle \sigma} \left(\hat{c}^\dagger_{\mathbf{j}\sigma} \hat{c}_{\mathbf{l}\sigma} + \hat{c}^\dagger_{\mathbf{l}\sigma} \hat{c}_{\mathbf{j}\sigma} \right) - \mu \sum_{\mathbf{j}} \left(\hat{n}_{\mathbf{j}\uparrow} + \hat{n}_{\mathbf{j}\downarrow} \right) \ . \tag{2}$$

$\hat{H}$ consists of a kinetic energy term which describes the destruction of a fermion of spin σ on site $\mathbf{l}$, via the operator $\hat{c}_{\mathbf{l}\sigma}$, and its re-creation on site $\mathbf{j}$, via the operator $\hat{c}^\dagger_{\mathbf{j}\sigma}$; and a chemical potential term. The creation and destruction operators obey anticommutation relations $\{\hat{c}^\dagger_{\mathbf{j}\sigma}, \hat{c}^\dagger_{\mathbf{l}\sigma'}\} = \{\hat{c}_{\mathbf{j}\sigma}, \hat{c}_{\mathbf{l}\sigma'}\} = 0$ and $\{\hat{c}_{\mathbf{j}\sigma}, \hat{c}^\dagger_{\mathbf{l}\sigma'}\} = \delta_{\mathbf{j}\mathbf{l}} \delta_{\sigma\sigma'}$, which guarantee that they describe fermionic particles. As one consequence, the number operators $\hat{n}_{\mathbf{j}\sigma} = \hat{c}^\dagger_{\mathbf{j}\sigma} \hat{c}_{\mathbf{j}\sigma}$ can take only the values $0, 1$.

The symbol $\langle \mathbf{j}, \mathbf{l} \rangle$ in Eq. (2) denotes the collection of pairs of sites between which the hopping of electrons is allowed. Very commonly, this is restricted to the near neighbor sites of some periodic lattice, for example a one-dimensional chain, two dimensional square, triangular, or honeycomb lattice, etc. Because there are no interactions, the two spin species $\sigma = \uparrow, \downarrow$ can, for the moment, be considered independently. We will define the density ρ to be the number of fermions per lattice site.

For most of this chapter, we will assume periodic boundary conditions. In this situation, the translation invariance of the geometry suggests that going to momentum space will simplify our understanding. Indeed, if we introduce

$$\hat{c}^\dagger_{\mathbf{k}\sigma} = \frac{1}{\sqrt{N}} \sum_{\mathbf{j}} e^{+i\mathbf{k}\cdot\mathbf{j}} \hat{c}^\dagger_{\mathbf{j}\sigma} \qquad\qquad \hat{c}^\dagger_{\mathbf{j}\sigma} = \frac{1}{\sqrt{N}} \sum_{\mathbf{k}} e^{-i\mathbf{k}\cdot\mathbf{j}} \hat{c}^\dagger_{\mathbf{k}\sigma} \ , \tag{3}$$

the Hamiltonian Eq. (2) becomes diagonal: rather than destruction on one spatial site being partnered with creation on a *different* spatial site, creation and destruction processes only occur between *identical* momenta. It is worth emphasizing that the new 'momentum creation and destruction operators' obey the same anti-commutation relations of the original operators in real space, so that each of the momenta states $\mathbf{k}$ can be occupied by at most one fermion of each spin species.

Let's consider, for concreteness, a one dimensional chain. The explicit calculation is (ignoring

the chemical potential term)

$$
\begin{aligned}
\hat{H} &= -t \sum_{j,\sigma} \left(\hat{c}_{j\sigma}^{\dagger} \hat{c}_{j+1\sigma} + \hat{c}_{j+1\sigma}^{\dagger} \hat{c}_{j\sigma} \right) \\
&= -\frac{t}{N} \sum_{j,\sigma} \sum_{k} \sum_{k'} \left(e^{-ikj} \hat{c}_{k\sigma}^{\dagger} e^{+ik'(j+1)} \hat{c}_{k'\sigma} + e^{-ik(j+1)} \hat{c}_{k\sigma}^{\dagger} e^{+ik'j} \hat{c}_{k'\sigma} \right) \\
&= -\frac{t}{N} \sum_{k} \sum_{k'} \sum_{j\sigma} e^{+i(k'-k)j} \left(e^{+ik'} + e^{-ik} \right) \hat{c}_{k\sigma}^{\dagger} \hat{c}_{k'\sigma} .
\end{aligned}
\tag{4}
$$

If we use the orthogonality relation $\sum_{j} e^{+i(k'-k)j} = N\delta_{kk'}$ (which is also employed in the inversion of the site to momentum transformation of Eq. (3)) we obtain the Hamiltonian in momentum space

$$
\hat{H} = \sum_{k\sigma} -2t \cos k \; \hat{c}_{k\sigma}^{\dagger} \hat{c}_{k\sigma} .
\tag{5}
$$

The structure of Eq. (5) is quite general, that is, also correct in higher dimension and on different lattice structures. For an arbitrary TBH,

$$
\hat{H} = \sum_{\mathbf{k}\sigma} \varepsilon_{\mathbf{k}} \, \hat{n}_{\mathbf{k}\sigma} \qquad\qquad \hat{n}_{\mathbf{k}\sigma} = \hat{c}_{\mathbf{k}\sigma}^{\dagger} \hat{c}_{\mathbf{k}\sigma} .
\tag{6}
$$

As noted earlier, $\hat{H}$ is diagonal in the momentum indices, so that a state characterized by the occupation of certain momenta is an eigenstate of $\hat{H}$ with an energy equal to the sum of the corresponding $\varepsilon_{\mathbf{k}}$. This is, obviously, not true of position occupation number states. Different lattice geometries are encapsulated in the specific dispersion relation $\varepsilon_{\mathbf{k}}$. Summarizing, then, when viewed in momentum space there is a single, continuous, 'energy band' which is, at $T = 0$ occupied by two, spin $\uparrow$ and $\downarrow$, fermions for all $\varepsilon_{\mathbf{k}} < \mu$. Such a model is always metallic, except, at zero temperature T, in the trivial limits where μ is below the lowest level in the band, i.e., when there are no fermions on the lattice ($\rho = 0$) or when μ is above the highest level in the band, i.e., when every level is occupied ($\rho = 2$).

A more interesting situation arises when multiple energy bands are present. This can occur in a variety of ways. Again focussing on a one dimensional chain, consider an additional staggered potential $\Delta \sum_{j} (-1)^{j} n_{j\sigma} = e^{i\pi j} n_{j\sigma}$ in the Hamiltonian. When one goes to momentum space the staggered potential mixes momenta k and $k + \pi$:

$$
\Delta \sum_{j} (-1)^{j} c_{j}^{\dagger} c_{j} = \Delta \frac{1}{N} \sum_{j} \sum_{k} \sum_{p} e^{i\pi j} e^{-ikj} c_{k}^{\dagger} e^{+ipj} c_{p} = \Delta \sum_{k} c_{k}^{\dagger} c_{k+\pi} .
\tag{7}
$$

(We have used the orthogonality relation $\sum_{j} e^{+i(p+\pi-k)j} = N\delta_{k\,p+\pi}$ again.) Now, going to momentum space has not fully diagonalized the Hamiltonian: the wavevectors k and $k + \pi$ mix. Using the forms already written down for the hopping term,

$$
H = \sum_{k} \begin{pmatrix} c_{k}^{\dagger} & c_{k+\pi}^{\dagger} \end{pmatrix} \begin{pmatrix} -2t \cos k & \Delta \\ \Delta & -2t \cos (k+\pi) \end{pmatrix} \begin{pmatrix} c_{k} \\ c_{k+\pi} \end{pmatrix} ,
\tag{8}
$$
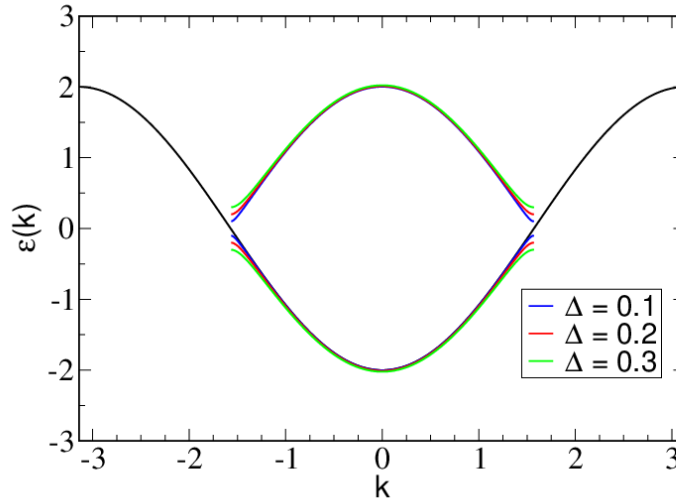
Fig. 1: *The dispersion relation of a one dimensional non-interacting TBH before (black) and after (red, blue, green) a staggered potential $(-1)^j \, \hat{n}_j$ is added. The staggered potential opens a gap near $k = \pm\pi/2$ and leads to insulating behavior at half-filling.*

where the k sum is over the reduced Brillouin zone $-\pi/2 < k < \pi/2$, so as not to overcount the modes.

This structure is not restricted to a one dimensional chain, but will arise for any 'bipartite' lattice (that is, one whose sites divide into two sets $\mathcal{A}$ and $\mathcal{B}$ such that the neighbors of $\mathcal{A}$ belong only to $\mathcal{B}$ and *vice-versa*. In this general situation, momenta $\mathbf{k}$ and $\mathbf{k} + \vec{\pi}$ mix. One must still do a final diagonalization of the 2x2 matrices in Eq. (8). The allowed energy levels are

$$E_{\mathbf{k}} = \pm\sqrt{\varepsilon_{\mathbf{k}}^2 + \Delta^2} \, , \tag{9}$$

where $\mathbf{k}$ ranges only over the reduced Brillouin zone containing only one of each pair $\mathbf{k}$ and $\mathbf{k} + \vec{\pi}$. The dispersion relation of Eq. (9) has a gap 2Δ separating the positive and negative $E_{\mathbf{k}}$. The system is insulating, not just in the trivial limits when there are no electrons on the lattice or when all sites are fully occupied, but also at half-filling $\rho = 1$, which occurs when the chemical potential $-2\Delta < \mu < +2\Delta$. See Fig. 1

One way of diagnosing such a band insulator is by computing $\rho(\mu)$. Within an energy band, the density ρ increases as the chemical potential μ is raised. However, for μ in the gap, ρ is constant. This plateau in $\rho(\mu)$ reflects a vanishing of the electronic compressibility $\kappa = \partial\rho/\partial\mu = 0$. We will see that this criterion for insulating behavior applies also to interaction-driven situations, but not to the disorder-induced Anderson insulator.

In the discussion above we generated multiple bands and a band gap through an additional staggered potential. One could also generalize the original TBH, Eq. (2), so that several fermionic species are present. One can, for example, allow two orbitals (and associated operators $\hat{c}$ and $\hat{d}$) on every site of a square lattice,

$$
\begin{aligned}
\hat{H} = -\, t \sum_{\langle \mathbf{j},\mathbf{l} \rangle \, \sigma} (\, \hat{c}_{\mathbf{j}\sigma}^\dagger \hat{c}_{\mathbf{l}\sigma} + \hat{c}_{\mathbf{l}\sigma}^\dagger \hat{c}_{\mathbf{j}\sigma} \,) - t \sum_{\langle \mathbf{j},\mathbf{l} \rangle \, \sigma} (\, \hat{d}_{\mathbf{j}\sigma}^\dagger \hat{d}_{\mathbf{l}\sigma} + \hat{d}_{\mathbf{l}\sigma}^\dagger \hat{d}_{\mathbf{j}\sigma} \,) \\
-\, t' \sum_{\mathbf{j}\,\sigma} (\, \hat{d}_{\mathbf{j}\sigma}^\dagger \hat{c}_{\mathbf{j}\sigma} + \hat{c}_{\mathbf{j}\sigma}^\dagger \hat{d}_{\mathbf{j}\sigma} \,) - \mu \sum_{\mathbf{j}} (\hat{n}_{\mathbf{j}\uparrow}^d + \hat{n}_{\mathbf{j}\downarrow}^d + \hat{n}_{\mathbf{j}\uparrow}^c + \hat{n}_{\mathbf{j}\downarrow}^c) \, . \tag{10}
\end{aligned}
$$

Each of the individual fermionic species associated with operators $\hat{c}$ and $\hat{d}$ hops on near-neighbor sites. However, the two types of fermions are also allowed to interconvert on the same site of the lattice, with hopping parameter t'.

Once again going to momentum space, the mixing of the two fermionic species leads to

$$\hat{H} = \sum_{\mathbf{k}\sigma} \varepsilon_{\mathbf{k}} \hat{c}_{\mathbf{k}\sigma}^\dagger \hat{c}_{\mathbf{k}\sigma} + \sum_{\mathbf{k}\sigma} \varepsilon_{\mathbf{k}} \hat{d}_{\mathbf{k}\sigma}^\dagger \hat{d}_{\mathbf{k}\sigma} + t' \sum_{\mathbf{k}\sigma} \left(\hat{d}_{\mathbf{k}\sigma}^\dagger \hat{c}_{\mathbf{k}\sigma} + \hat{c}_{\mathbf{k}\sigma}^\dagger \hat{d}_{\mathbf{k}\sigma} \right)$$
$$= \sum_k \left(\begin{array}{cc} c_{\mathbf{k}}^\dagger & d_{\mathbf{k}}^\dagger \end{array} \right) \left(\begin{array}{cc} \varepsilon_{\mathbf{k}} & t' \\ t' & \varepsilon_{\mathbf{k}} \end{array} \right) \left(\begin{array}{c} c_{\mathbf{k}} \\ d_{\mathbf{k}} \end{array} \right) . \tag{11}$$

The final 2x2 rotation yields the energy levels,

$$E_{\mathbf{k}}^\pm = -2t \left(\cos k_x + \cos k_y \right) \pm t' . \tag{12}$$

This band structure is somewhat more rich than that which arises from a staggered potential, where a gap opens for *any* nonzero Δ. Here, instead, the bands overlap for $t' < 4t$ and the system is always metallic (except for $\rho = 0$ or $\rho = 2$). However, it can be made insulating at $\rho = 1$ if $t' > 4t$. The TBH of Eq. (10) is sometimes used to describe 'bilayer' geometries, where c and d label two different spatial layers, as opposed to distinct orbitals.

The considerations of this section have described the simplest type of metal-insulator transition: Fermions which are noninteracting, on a translationally invariant lattice such that the placement of the chemical potential either within one of the energy bands (a metal) or in a gap between them (insulator).

3 Antiferromagnetic and charge density wave insulators

Insulating behavior which is closely connected, from the viewpoint of mathematical structure, to that of the previous section arises when interactions are included within mean-field theory (MFT). Consider the most simple type of TBH interaction, a repulsion between spin up and spin down fermions on the same spatial site. Together with the kinetic energy of Eq. (2) we obtain the Hubbard Hamiltonian,

$$\hat{H} = -t \sum_{\langle \mathbf{j},\mathbf{l} \rangle \sigma} \left(\hat{c}_{\mathbf{j}\sigma}^\dagger \hat{c}_{\mathbf{l}\sigma} + \hat{c}_{\mathbf{l}\sigma}^\dagger \hat{c}_{\mathbf{j}\sigma} \right) - \mu \sum_{\mathbf{j}} \left(\hat{n}_{\mathbf{j}\uparrow} + \hat{n}_{\mathbf{j}\downarrow} \right) + U \sum_{\mathbf{j}} \hat{n}_{\mathbf{j}\uparrow} \hat{n}_{\mathbf{j}\downarrow} . \tag{13}$$

The MFT approximation consists of recasting the interaction term in Eq. (13) as,

$$U \sum_{\mathbf{j}} \left(\hat{n}_{\mathbf{j}\uparrow} \langle \hat{n}_{\mathbf{j}\downarrow} \rangle + \hat{n}_{\mathbf{j}\uparrow} \langle \hat{n}_{\mathbf{j}\downarrow} \rangle - \langle \hat{n}_{\mathbf{j}\uparrow} \rangle \langle \hat{n}_{\mathbf{j}\downarrow} \rangle \right) . \tag{14}$$

It is clear that if the fermionic occupations possess an antiferromagnetic (AF) pattern, $\langle \hat{n}_{\mathbf{j}\uparrow} \rangle = \rho + (-1)^{\mathbf{j}} m$ and $\langle \hat{n}_{\mathbf{j}\downarrow} \rangle = \rho - (-1)^{\mathbf{j}} m$, on a bipartite lattice, then a staggered potential similar to that described by Eq. (7) is present. As a consequence of this 'spin density wave' (SDW), a band gap opens and 'Slater' insulating behavior arises, in direct analogy of the argument leading up to Eq. (8).

Although this MFT treatment of the Slater insulator is indeed close to that of a staggered potential, it is worth emphasizing that AF can also arise away from $\rho = 1$. Of course, it is necessary to determine whether the *ansatz* for $\langle n_{\mathbf{j}\sigma} \rangle$ in which the occupations vary spatially actually lowers the free energy for nonzero m. The answer will depend, in general, on U and ρ and can be used to generate the MFT phase diagram. The result for the $d = 2$ square lattice is given in [2]. Note that it is also possible that a 'ferromagnetic' *ansatz* $\langle \hat{n}_{\mathbf{j}\uparrow} \rangle = \rho + m$ and $\langle \hat{n}_{\mathbf{j}\downarrow} \rangle = \rho - m$, lowers the energy. This is quite a bit less likely to lead to an insulating gap since, as discussed above within the context of a bilayer model, a large order parameter m is required to introduce a gap between energy bands which are rigidly shifted, whereas a gap immediately opens for any staggered potential amplitude Δ.

A similar type of insulator arises when fermions interact with local phonon (oscillator) modes $\hat{p}_{\mathbf{j}}, \hat{q}_{\mathbf{j}}$, rather than with each other, *e.g.* in the Holstein model

$$\hat{H}_{\text{Holstein}} - t \sum_{\langle \mathbf{j}, \mathbf{l} \rangle \sigma} (\hat{c}_{\mathbf{j}\sigma}^{\dagger} \hat{c}_{\mathbf{l}\sigma} + \hat{c}_{\mathbf{l}\sigma}^{\dagger} \hat{c}_{\mathbf{j}\sigma}) + \frac{1}{2} \sum_{\mathbf{j}} (\hat{p}_{\mathbf{j}}^2 + \omega^2 \hat{q}_{\mathbf{j}}^2) + \lambda \sum_{\mathbf{j}} (\hat{n}_{\mathbf{j}\uparrow} + \hat{n}_{\mathbf{j}\uparrow}) \, \hat{q}_{\mathbf{j}} \; . \quad (15)$$

One can get a preliminary understanding of its physics by ignoring the phonon kinetic energy and considering only static ionic displacements. On a bipartite lattice, an oscillating set of displacements $\langle \hat{q}_{\mathbf{j}} \rangle = q_0 (-1)^{\mathbf{j}}$ opens a gap in the fermion dispersion relation precisely as with a staggered potential associated with an AF spin pattern. Unlike the latter case, however, the resulting densities of up and down spin are in phase, leading to a charge density wave (CDW) as opposed to a SDW. At half-filling, the lowering of the electronic energy from $\varepsilon_{\mathbf{k}}$ to $E_{\mathbf{k}} = -\sqrt{\varepsilon_{\mathbf{k}}^2 + \Delta^2}$ favors non-zero values of q_0. Against this competes the increase in the potential energy $\omega_0^2 q_0^2 / 2$. Which effect dominates depends on the phonon frequency ω_0, the electron-phonon coupling λ, the dimensionality of the lattice, and, of course, a proper treatment of quantum fluctuations of the phonons.

4 Anderson and Mott insulators

In this section we combine a discussion of two distinct types of insulator, those arising from disorder and those arising from strong repulsive interactions.

Anderson insulators develop from randomness in a tight binding Hamiltonian. We begin our discussion by considering a one dimensional TBH with a single site at the chain center $N/2$ with a lower energy than all the others

$$\hat{H} = -t \sum_{j,\sigma} (\hat{c}_{j\sigma}^{\dagger} \hat{c}_{j+1\,\sigma} + \hat{c}_{j+1\,\sigma}^{\dagger} \hat{c}_{j\sigma}) - \mu_0 \, c_{N/2,\sigma}^{\dagger} c_{N/2,\sigma} \; . \quad (16)$$

Figure 2(top left) shows the eigenenergies, obtained numerically by diagonalizing $\hat{H}$. Since translation invariance is broken by the impurity, we no longer label the eigenvalues with a momentum index k. Nevertheless, all but one of the eigenvalues form a band, which looks very much like the $\varepsilon(k) = -2t \cos(k)$ in the absence of the impurity ($\mu_0 = 0$). However, there is one extremal eigenvalue split off from all the others, which we have placed at $n = 512$. This
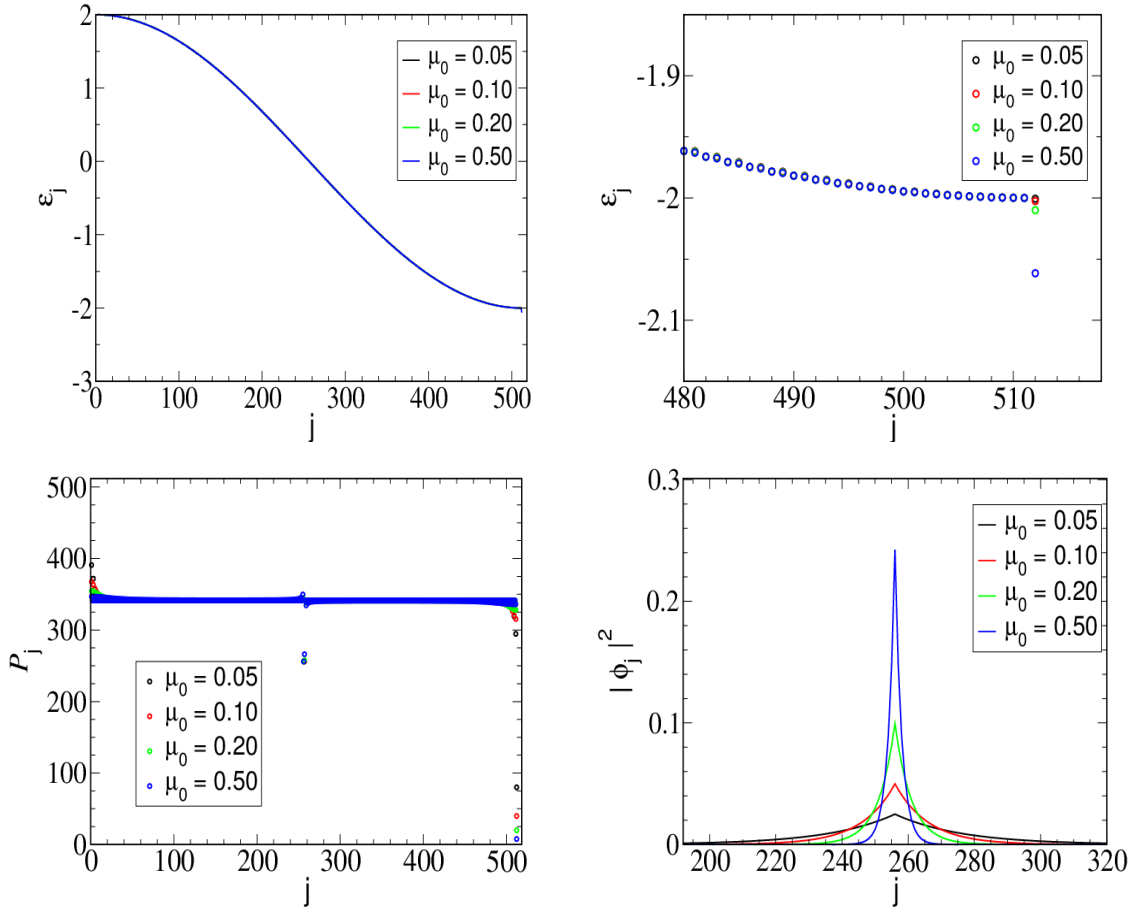
Fig. 2: *Top Left: Eigenspectrum of the TBH Eq.* (16) *for a chain of length* $N = 512$ *and impurity depths* $\mu_0 = 0.05, 0.10, 0.20, 0.50$. *Shown over their full range, the energy levels are indistinguishable from each other and from those of Fig. 1. Top Right: A blow-up of the eigenspectrum allows the resolution of the impurity level split off below the energy band. Bottom Left: Participation ratios of all eigenvectors are of order the number of sites* N, *except for the single, localized mode. Bottom Right: The square of the components of the associated eigenfunctions, in the vicinity of the defect at* $N/2 = 256$. *As the impurity depth* μ_0 *decreases, the eigenfunctions are less localized. Since momentum is no longer a good quantum number in the presence of the breaking of translation invariance by the defect, the horizontal axes in the top row are labeled by the eigenvalue index* j *rather than* k.

separation is clear in the blow up of Fig. 2(top right). Figure 2(bottom right) plots the square of the amplitude of the components $\left| \phi_j \right|^2$ of the localized eigenfunctions. They are seen to be sharply peaked at $N/2$.

A useful way to characterize the spatial extent of an eigenfunction with components ϕ_j (which we assume are normalized to $\sum_j \left| \phi_j \right|^2 = 1$) is via the participation ratio $\mathcal{P}$

$$\mathcal{P}^{-1} = \sum_j \left| \phi_j \right|^4. \tag{17}$$

If the eigenfunction is fully localized on a single site j_0, that is, if $\phi_j = \delta(j, j_0)$, it is easy to see $\mathcal{P}^{-1} = 1$ and hence $\mathcal{P} = 1$. On the other hand, if the eigenfunction is completely delocalized $\phi_j = 1/\sqrt{N}$ we have $\mathcal{P}^{-1} = 1/N$ and hence $\mathcal{P} = N$. By considering other cases one can

be convinced that, roughly speaking, $\mathcal{P}$ measures the number of sites in the lattice where ϕ_j is "large." Figure 2(bottom left) plots these participation ratios. They are all of the order of the lattice size N (meaning the states are delocalized) except for a single mode ($j = 512$) which is localized.

This problem is formally very similar to that of localization of vibrations of a harmonic chain with a single mass m' or spring k' which differs from all the others, in the sense that the solution of both reduces to diagonalization of the same type of matrices. In the case of vibrations, it is interesting to note that localization occurs only for a defect mass which is *lighter* than all the others. This can be seen to be physically reasonable in the extreme limits: If $m' \ll m$, one pictures the very light mass as vibrating back and forth between the heavy 'walls' provided by its neighbors. A heavy defect, $m' \gg m$, shoves aside its neighbors and its vibrations spread throughout the chain.

The problem of a small number of impurities in a noninteracting TBH can be treated analytically [3]. The procedure is sufficiently interesting and important to provide the initial steps here. In order to connect this discussion with the previous material, it is useful to recall an alternate approach to the solution of noninteracting TBHs.

We solved Eq. (2) by a rather sophisticated method, namely by doing a canonical transformation on the fermionic creation and annihilation operators which diagonalized $\hat{H}$. A less sophisticated solution is to construct the matrix for $\hat{H}$ using position occupation states as a basis. This is done in the usual way, by allowing $\hat{H}$ to act on each basis vector. Because $\hat{H}$ conserves particle number (fermion creation and destruction operators always appear as partners), its matrix consists of independent blocks corresponding to the particle number. For a linear chain of N sites with periodic boundary conditions, then

$$
\begin{aligned}
\hat{H} \, | \, 1\,0\,0\,0\,0\,0\cdots 0\,0 \, \rangle &= -t \, | \, 0\,1\,0\,0\,0\,0 \cdots 0\,0 \, \rangle - t \, | \, 0\,0\,0\,0\,0\,0 \cdots 0\,1 \, \rangle \\
\hat{H} \, | \, 0\,1\,0\,0\,0\,0\cdots 0\,0 \, \rangle &= -t \, | \, 1\,0\,0\,0\,0\,0 \cdots 0\,0 \, \rangle - t \, | \, 0\,0\,1\,0\,0\,0 \cdots 0\,0 \, \rangle \\
\hat{H} \, | \, 0\,1\,0\,0\,0\,0\cdots 0\,0 \, \rangle &= -t \, | \, 1\,0\,0\,0\,0\,0 \cdots 0\,0 \, \rangle - t \, | \, 0\,0\,1\,0\,0\,0 \cdots 0\,0 \, \rangle
\end{aligned}
$$
$$
\cdots \text{etc.} \tag{18}
$$

The calculation of the single particle eigenstates ϕ and eigenenergies E, in the absence of an impurity, therefore corresponds to the linear algebra problem,

$$
\sum_n L_{mn} \, \phi_n = 0 \qquad L_{mn} = E \, \delta_{mn} - t \, \delta_{m,n-1} - t \, \delta_{m,n+1} \; , \tag{19}
$$

where L is the matrix of numbers which forms the single particle block of $\hat{H}$ in the occupation number basis.

The nontrivial solution of Eq. (19) requires the vanishing of the determinant $| \, L \, | = 0$. It is an easily proven that the k component of the nth eigenvector is $\phi_n = e^{ikn}$, and $E_k = -2\,t\cos k$, solve Eq. (19). The periodic boundary conditions discretize the allowed k values to $k = 2\pi n/N$ with $n = \{1, 2, 3, \ldots, N\}$. Notice that this solution is precisely the same as that arising from the transformation to momentum space operators, Eq. (5)!
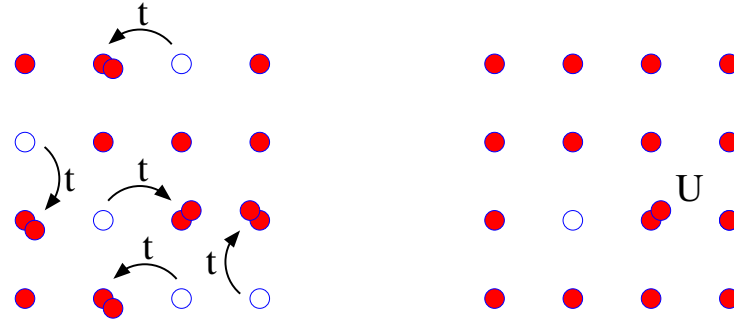
Fig. 3: *The qualitative physics of the Mott insulator is seen by considering a half-filled system (one particle per site). <u>Left</u>: When the on-site repulsion U between particles is weak, they are free to hop around the lattice. Empty, singly, and doubly occupied sites are all present, with only the average density equalling one particle per site. <u>Right</u>: On the other hand, when U is very large compared to t, it is energetically preferable for the particles to sit with exactly one fermion on each individual site.*

This second approach to the problem lends itself nicely to an attack on the behavior in the presence of randomness. One can write the problem as,

$$\sum_n L_{mn}\,\phi_n = \sum_k \delta L_{mk}\,\phi_k \qquad \rightarrow \qquad \big(I - G\,\delta L\big)\,\phi = 0\ , \tag{20}$$

where δL is the matrix which contains the local chemical potentials and $G = L^{-1}$. In the case of Eq. (16), δL has a single nonzero entry along its diagonal.

A solution to Eq. (20) is,

$$\phi_n = \sum_{lk} G_{nl}\,\delta L_{lk}\,\phi_k\ . \tag{21}$$

However, this a only 'formal' solution because the unknown variables ϕ_n appear on both sides of Eq. (21). However, note that the non-trivial solution of Eq. (21) requires $|\,I - G\,\delta L\,| = 0$. The important observation is that the sparsity or δL enormously simplifies the linear algebra problem. Instead of rank N, the matrix $I - G\,\delta L$ whose determinant must be computed has much lower rank. Furthermore, the solution of the eigenproblem of L is known, we have an explicit expression for the Green function, $G_{nl} = \sum_k e^{ik(n-l)}/E_k$. Amazingly, then, the problem of the modes in the presence of $n \ll N$ defects boils down to the diagonalization of an $n \times n$ matrix, whose elements involve the known defect potential δL and Green function G. Ref. [3] provides some explicit examples, and a beautiful graphical solution of several interesting cases.

Having discussed the situation when there is a single, or small number of, defects, it is natural to ask what happens when there are many impurities present, for example when there is a randomly chosen chemical potential on *every* site of the lattice. This is the problem of 'Anderson Localization' [4]. In one dimension, all the eigenstates become localized, for any amplitude of disorder. This is also true in two dimensions, although just barely [5]. In three dimensions, the eigenfunctions at the extremes of the spectrum (that is, those associated with the largest and
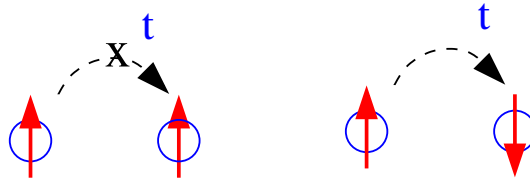
Fig. 4: *The Pauli Principle prevents fermions of like spin on adjacent sites from hopping (left), a process which is allowed if the fermions have opposite spin (right). In the case of antiparallel spin, the intermediate state created by the hop has a doubly occupied site, and hence a potential energy U. The resulting second order lowering of the energy relative to the parallel spin arrangement is proportional to $-t^2/U$.*

smallest eigenvalues) are localized, while the eigenfunctions near the center of the spectrum are extended. The energy which separates these two behaviors is referred to as the mobility edge.

In 3D one has the appearance of Anderson insulating behavior, and the possibility of associated metal-insulator transitions: If the chemical potential lies below the mobility edge, only localized eigenfunctions are occupied, and the system is an insulator. When μ crosses the mobility edge, extended states become occupied, and the system becomes a metal. It is important to emphasize that, in stark contrast to the band, SDW, and CDW insulators previously discussed, there is *no gap* in the spectrum. The compressibility κ is nonzero in the insulator, and a plot of density ρ as a function of chemical potential μ would show no marked signal at the transition from Anderson insulator to metal.

The final qualitative discussion concerns "Mott insulators," whose behavior arises from inter-actions, as opposed to gaps in the band structure or localization by disorder. Consider a single band Hubbard Hamiltonian, for example on a square lattice, at "half-filling" (one electron per site). The simple physical picture of a Mott insulator is that if the on-site repulsion U is very large, the energy cost for the double occupation which must occur in order for the electrons to move, overwhelms the kinetic energy and freezes the electrons in place. See Fig. 3.

Although in Fig. 3 the spin orientations of the fermions are not indicated, it is natural to ask if they have any preferred arrangement. There are several arguments which suggest AF order. The first treats the hopping term in the Hubbard Hamiltonian Eq. (13) perturbatively. Consider two adjacent sites, both singly occupied with fermions of parallel spin. The interaction energy is zero, and, because of the Pauli Principle, the matrix element of the kinetic energy in this state vanishes, so there is no shift in the energy. If the fermions have antiparallel spin, however, the kinetic energy operator connects to an intermediate state with one empty and one doubly occupied site, with energy U. Thus the energy of a pair of sites with antiparallel spin fermions is lowered by $\Delta E \sim -t^2/U$. See Fig. 4. There are other arguments suggesting AF dominates at half-filling, for example a calculation of the magnetic susceptibility of the Hubbard Hamiltonian within the random phase approximation. A very nice early discussion of these ideas, emphasizing several unique features of the square lattice dispersion, is contained in Ref. [2].

Figure 5 shows some quantum simulation results for the square lattice Hubbard Hamiltonian at $U = 4$. $\rho(\mu)$ develops a 'Slater-Mott' plateau at half-filling. (See below.) The figure uses a convention in which the interaction term is written in particle-hole symmetric form so that
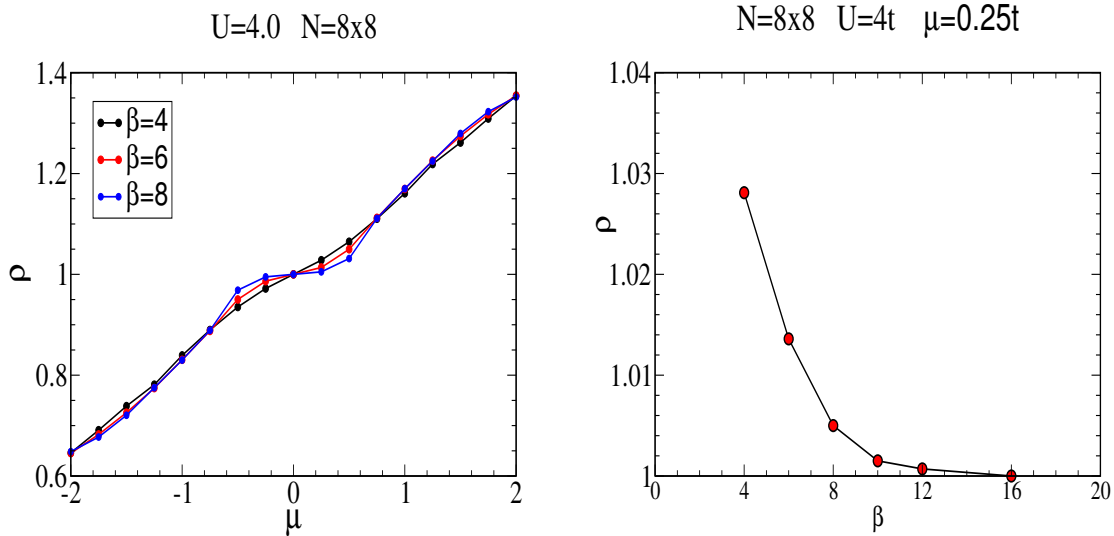
Fig. 5: _Left: The density ρ as a function of the chemical potential μ for the Hubbard Hamiltonian on a square lattice at $U = 4t$ and three different inverse temperatures $\beta = t/T = 4, 6, 8$. As β increases, Right: The density of fermions at a nonzero chemical potential, as a function of β shows that $\rho \to 1$._

$\mu = 0$ corresponds to $\rho = 1$. The vanishing of the compressibility, $\kappa = 0$, at $\rho = 1$ is a truly remarkable change in behavior since, on the square lattice, the noninteracting system has a divergent density of states at half-filling: $\kappa = \infty$ at $U = 0$! The algorithm used in the figure is 'determinant QMC'. This approach treats the interactions between electrons exactly, on lattices of finite spatial extent (a few hundred up to about a thousand spatial sites), and thus provides a much more rigorous treatment than that provided by MFT. The reader is referred to Refs. [2, 6–8] for a discussion of DQMC and its application to magnetism in the 2D Hubbard Hamiltonian.

The review of these ideas emphasizes an important point: in many situations (especially on bipartite lattices) a 'Slater insulator,' which occurs at weak to intermediate U due to the opening of an AF gap, merges smoothly, as U increases, into the Mott insulator where the lack of transport predominantly arises from the high cost of double occupancy. There is no sharp boundary between these two types of insulator, but rather a gradual crossover. A very deep question indeed is whether for fermionic systems symmetry breaking such as AF order always accompanies the Mott insulator, or whether a featureless, translationally invariant Mott phase can occur, as for collections of bosonic particles [9].

5   Formal definitions

The proverbially alert reader will have noticed that the preceding discussion avoided what would seemingly be the most natural quantity to distinguish metals and insulators, namely the conductivity σ. This is because transport properties are a bit more subtle to deal with. We will now consider σ and develop an understanding, which unifies the preceding, more qualitative, discussion. An added bonus will be the fact that the superfluid density, the defining characteristic

of a superconductor, naturally arises. The discussion in this section very closely follows that of Ref. [1]. The derivation is a bit dense. The key 'practical results' are Eqs. (30) and (31) which allow for the determination of Drude weight D and superfluid density D_s from the current-current correlation function Λ_{xx}.

Consider the response of the current to presence of a vector potential $A_x(\mathbf{l})$. As shown in Ref. [10], this modifies the hopping term in the kinetic energy (suppressing the spin indices),

$$c^\dagger_{\mathbf{l}+x}c_{\mathbf{l}} + c^\dagger_{\mathbf{l}}c_{\mathbf{l}+x} \rightarrow e^{ieA_x(\mathbf{l})}c^\dagger_{\mathbf{l}+x}c_{\mathbf{l}} + e^{-ieA_x(\mathbf{l})}c^\dagger_{\mathbf{l}}c_{\mathbf{l}+x} \; . \tag{22}$$

This can be expanded in powers of A so that the kinetic energy K acquires an additional term which can be expressed in terms of the paramagnetic current density in the x direction $ej^p_x(\mathbf{l})$ and the kinetic energy density on bonds in the x direction, $k_x(\mathbf{l})$,

$$K_A = K - \sum_{\mathbf{l}} \left(ej^p_x(\mathbf{l})A_x(\mathbf{l}) + \frac{e^2 k_x(\mathbf{l})}{2} A_x(\mathbf{l})^2 \right) \tag{23}$$

$$j^p_x(\mathbf{l}) = it \sum_\sigma \left(c^\dagger_{\mathbf{l}+x\,\sigma}c_{\mathbf{l}\,\sigma} - c^\dagger_{\mathbf{l}\,\sigma}c_{\mathbf{l}+x\,\sigma} \right)$$

$$k_x(\mathbf{l}) = -t \sum_\sigma \left(c^\dagger_{\mathbf{l}+x\,\sigma}c_{\mathbf{l}\,\sigma} + c^\dagger_{\mathbf{l}\,\sigma}c_{\mathbf{l}+x\,\sigma} \right) \; .$$

Differentiating Eq. (23) with respect to $A_x(\mathbf{l})$ yields the total current density, which includes both paramagnetic and diamagnetic contributions,

$$j_x(\mathbf{l}) = -\frac{\delta K_A}{\delta A_x(\mathbf{l})} = e\, j^p_x(\mathbf{l}) + e^2\, k_x(\mathbf{l})\, A_x(\mathbf{l}) \tag{24}$$

If one assumes a plane wave form for the vector potential,

$$A_x(\mathbf{l}, t) = \mathrm{Re}\left(A_x(\mathbf{q}, \omega)\, e^{i\mathbf{q}\cdot\mathbf{l} - i\omega t} \right) \; , \tag{25}$$

then the resulting current is,

$$\langle j_x(\mathbf{l}, t) \rangle = \mathrm{Re}\left(\langle\, j_x(\mathbf{q}, \omega) \rangle\, e^{i\mathbf{q}\cdot\mathbf{l} - i\omega t} \right)$$

$$\langle\, j_x(\mathbf{q}, \omega) \rangle = -e^2 \left(\langle k_x \rangle - \Lambda_{xx}(\mathbf{q}, \omega) \right) A_x(\mathbf{q}, \omega) \; . \tag{26}$$

The real-frequency current-current correlation functions $\Lambda(\mathbf{q}, \omega)$ are related to those at Matsubara frequencies $i\omega_m = 2\pi m T$,

$$\Lambda_{xx}(\mathbf{q}, i\omega_m) = \frac{1}{N} \int_0^\beta d\tau\, e^{i\omega_m \tau} \langle j^p_x(\mathbf{q}, \tau) j^p_x(-\mathbf{q}, 0) \rangle \; , \tag{27}$$

by analytic continuation.

Equations (26), (27) and the calculations leading to them are simply somewhat more complex versions of the relations such as the one which expresses the magnetization induced by an applied Zeeman field, to the magnetization-magnetization correlation functions and thereby the magnetic susceptibility χ, or any of the other multitude of 'fluctuation-dissipation' relations which arise from linear response theory.

It remains to connect this rather abstract quantity to more physical objects like the superfluid density: For bosonic particles, the superfluid density can be measured in, for example, a torsional oscillator experiment. As T is decreased below the superfluid transition temperature, the moment of inertia of a liquid in a container abruptly decreases, because the liquid inside no longer couples to the walls of the container. As we discuss below, for fermionic particles the superfluid density determines the distance to which a magnetic field penetrates a superconductor.

One of the early fundamental advances in understanding superconductivity was London's observation that the Meissner effect follows if one assumes the current density is proportional to the vector potential,

$$j_x(q_y) = -\frac{1}{4\pi}\frac{1}{\lambda^2}A_x(q_y) . \tag{28}$$

That is, magnetic fields will be expelled from a superconductor at distances beyond the penetration depth λ,

$$\frac{1}{\lambda^2} = \frac{4\pi n_s e^2}{mc^2} , \tag{29}$$

which depends on the superfluid density n_s. A comparison of Eqs. (28), (29) with Eq. (26) provides a link between the superfluid weight $D_s = n_s/m$ and the current-current correlation function:

$$\frac{D_s}{\pi e^2} = -\langle -k_x \rangle - \Lambda_{xx}(q_x = 0, q_y \to 0, i\omega_m = 0) . \tag{30}$$

The usual relations between vector potential and electric field, $E_x = -\partial A_x/\partial t$, and between the conductivity and electric field, result in an analogous formula for the Drude weight, the delta function contribution $D\delta(\omega)$ to the conductivity,

$$\frac{D}{\pi e^2} = -\langle -k_x \rangle - \Lambda_{xx}(q_x = 0, q_y = 0, i\omega_m \to 0) . \tag{31}$$

Details of this connection are in Ref. [1].

The third limit, in which the longitudinal momentum is taken to zero, relates Λ to the kinetic energy,

$$\langle -k_x \rangle = \Lambda_{xx}(q_x \to 0, q_y = 0, i\omega_m = 0) . \tag{32}$$

Summarizing, the key results are the following: Depending on the limits in which the momenta and frequency are taken to zero, one can obtain superfluid density D_s and Drude weight D from the current-current correlation function.

The superfluid density D_s and the Drude weight D form a basis for distinguishing an insulator ($D = D_s = 0$), from a metal, ($D \neq 0, D_s = 0$), from a superconductor ($D_s \neq 0$). It is rather remarkable that these alternate limits of approaching zero momentum and frequency yield distinct results and profoundly different physical quantities, especially to physicists who are accustomed to not being overly worried about the subtleties of the order of operations.

We will introduce the simplified notation $\Lambda^{\mathrm{L}} \equiv \lim_{q_x \to 0} \Lambda_{xx}(q_x, q_y = 0; i\omega_n = 0)$ and $\Lambda^T \equiv \lim_{q_y \to 0} \Lambda_{xx}(q_x = 0, q_y; i\omega_n = 0)$ so that Eqs. (30) and (32) can be simply expressed as $D_s = \pi[-K_x - \Lambda^T]$ and $-K_x = \Lambda^L$ respectively.
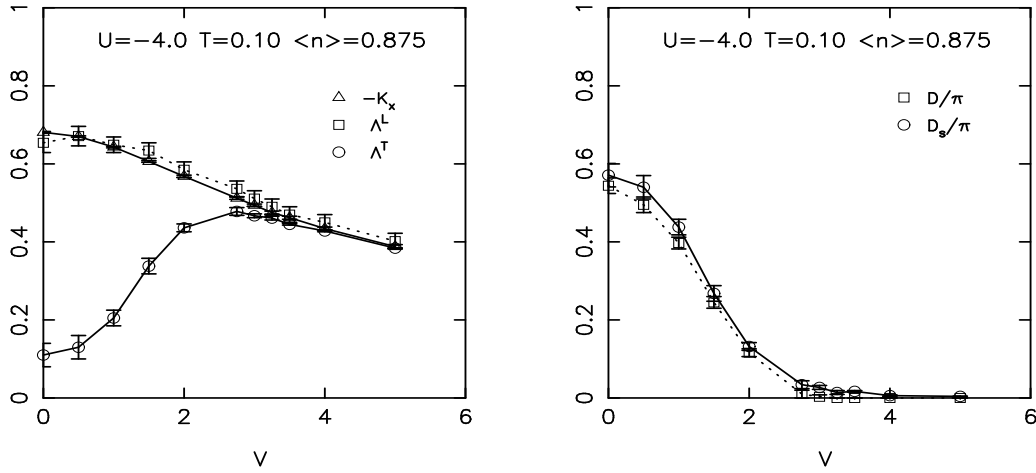
Fig. 6: _Left: Kinetic energy K_x, longitudinal Λ^L, and transverse Λ^T limits of current-current correlation function for the attractive Hubbard model with $U = -4\,t$ at temperature $T = 0.1$ and filling $\rho = 0.875$. The horizontal axis is the strength of random site energies $-V < \mu_i < +V$. The data indicate that $\Lambda^L = -K_x$ over all parameter ranges, as required by gauge invariance. Right: The superfluid density $D_s = \pi\left(-K_x - \Lambda^T\right)$ and Drude weight D. To within the accuracy of the numerics, $D = D_s$. See Eqs. (30), (31), and also Fig. 7_

6 Applications of formal theory

Ref. [1] considered the simplest TBHs to check their formalism, namely the clean, single band attractive and repulsive Hubbard Hamiltonians on a square lattice. Here we present results [11] on a TBH which also includes disorder in the site energies (an additional term $\sum_i v_i(n_{i\uparrow} + n_{i\downarrow})$ in the Hubbard Hamiltonian), to illustrate how powerful and general Eqs. (30), (31) truly are. We use the same DQMC approach which generated the data shown in Fig. 5 (and which was used in [1]). We note, however, that the implementation of these criteria within DQMC requires the evaluation of imaginary time-dependent observables, as opposed to the algorithmically more simple equal time quantities like the energy, density, and magnetic, charge, and pairing structure factors. Such calculations slow down DQMC simulations quite significantly, especially at low temperatures and on large spatial lattices.

It is important to note that, while the presence of randomness breaks translation invariance for a *single* disorder realization, translation invariance is recovered after disorder averaging. Typically one finds calculations for 10-100 distinct instances of the local site potential $\{v_i\}$ are required in DQMC simulations such as those described here.

Results from [11] for Λ^T, Λ^L and $-K_x$ are plotted in Fig. 6(left) as a function of the strength V of randomness in the site energies $-V < v_i < +V$. The attractive interaction strength $U = -4$, temperature $T = 0.10$, and density $\rho = 0.875$. D and D_s are plotted in Fig. 6(right). They decrease monotonically with disorder. There is a critical value V_c beyond which $D = D_s = 0$ and the system becomes insulating. These results are consistent with a direct superconductor to insulator transition in 2D, without an extended intervening metallic phase.

Figure 7 provides some numerical details on the extrapolation in Matsubara frequencies which, following Eq. (31), is needed to capture D. Similar plots showing the momentum extrapolations
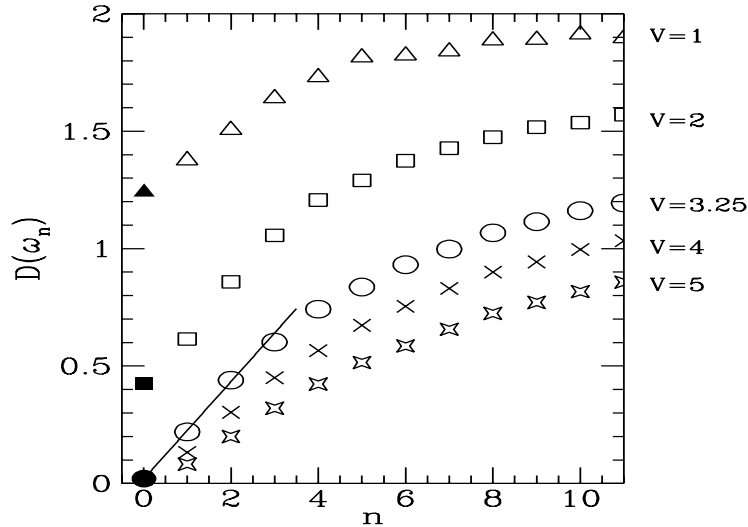
Fig. 7: *Illustration of the details of the extrapolation procedure to obtain the Drude weight D via Eq. (31). The horizontal axis $n = \omega_n/(2\pi T)$. Parameters are as in Fig. 6. In the metallic phase, which occurs precisely at the critical point $V = V_c \sim 3.25$, the slope of $D(\omega_n)$ can be used to obtain σ_{dc}. See text.*

to obtain D_s and verify $\Lambda^L = -\langle K_x \rangle$ are not shown, but can be found in Ref. [1]. Note that in general the simulations are performed in a regime where there are up to several hundred Matsubara frequencies, but only 10-30 momenta in each direction, an order of magnitude less. Thus the momentum extrapolations needed for Λ^L and Λ^T are typically more challenging than those for D.

As argued in Ref. [1], the extrapolation in Fig. 7 can also be used to obtain the dc conductivity via

$$D(\omega_n) = \pi \sigma_{dc} |\omega_n| \ . \tag{33}$$

We will use this as a consistency check against alternate ways of quantifying the metal-insulator transition and obtaining σ_{dc}.

7 Conductivity and spectral function

This final section before the conclusions will focus on two further QMC approaches to the metal-insulator transition. The first technique, like those of Sec. 6, begins with the current-current correlation function, but has the advantage of avoiding analytic continuation and extrapolation to zero momentum or frequency. It is, however, approximate. The second method moves away from Λ_{xx} and instead considers the spectral function.

Consider the fluctuation-dissipation theorem

$$\Lambda_{xx}(\mathbf{q}, \tau) = \int_{-\infty}^{+\infty} \frac{d\omega}{\pi} \frac{\exp(-\omega\tau)}{1 - \exp(-\beta\omega)} \operatorname{Im} \Lambda_{xx}(\mathbf{q}, \omega) \ . \tag{34}$$

In principle one can invert this Laplace transform to get $\operatorname{Im} \Lambda_{xx}$, but this process is known to be very ill-conditioned [12]. We instead proceed as follows: If the temperature $T \ll \Omega$, the scale
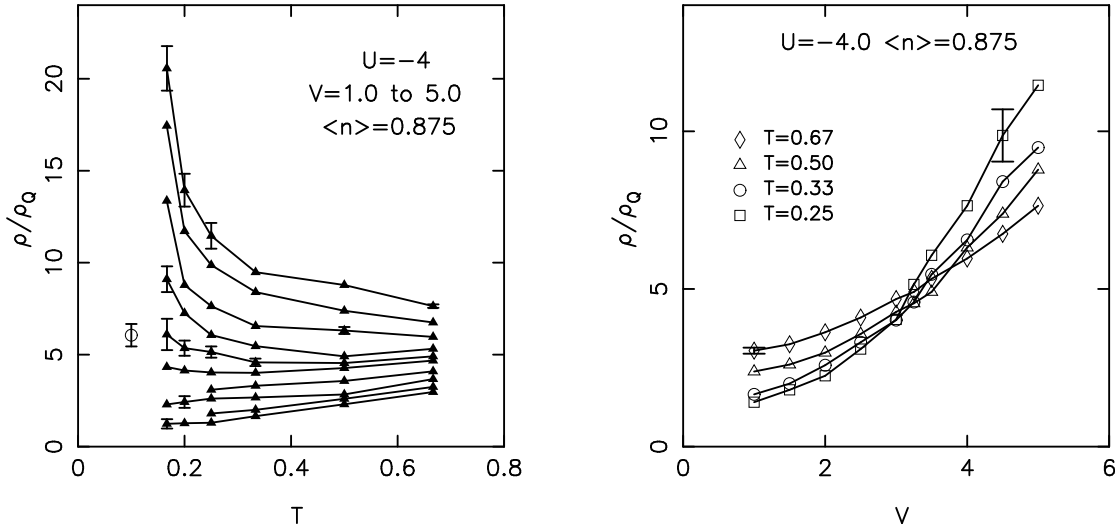
Fig. 8: *Left: The resistivity $\rho_{dc} = 1/\sigma_{dc}$ obtained from Eq. (35) as a function of temperature. The on-site attraction $U = -4\,t$ and the density $\rho = 0.875$. The curves are (top to bottom) for disorder strengths $V = 5.0, 4.5, 4.0, 3.5, 2.0, 2.5, 2.0, 1.5, 1.0$. For large V, ρ_{dc} increases as T is lowered, indicating insulating behavior. For small V, ρ_{dc} decreases as T is lowered, indicating metallic behavior. The open symbol at $T = 0.10$ is the value of ρ_{dc} inferred from the $V = V_c$ data in Fig. 7. See text. Right: The data are replotted to show ρ_{dc} as a function of V for curves of constant T. The crossing indicates the approximate position V_c of the metal-insulator transition. For these parameters, the superconducting transition temperature $T_c \lesssim 0.05t$, so no abrupt drop in ρ_{dc} occurs. The quantum of resistance $\rho_Q = h/(4e^2) = \pi/2$ in our units ($\hbar = e^2 = 1$).*

at which Im Λ deviates from its low frequency behavior Im $\Lambda \sim \omega\sigma_{dc}$, it is useful to evaluate Eq. (34) at the largest possible imaginary time, $\tau = \beta/2$. By doing this, the factor $e^{-\omega\tau}$ cuts off all contributions to the integral for frequencies above Ω, allowing us to replace Im Λ by $\omega\sigma_{dc}$, and enabling an analytic evaluation of the integral. The result

$$\sigma_{\mathrm{dc}} = \frac{\beta^2}{\pi}\Lambda_{xx}(\mathbf{q} = 0, \tau = \beta/2) , \tag{35}$$

provides a very useful approximate formula for σ_{dc}, subject to the restrictions noted above.

The reasoning leading to Eq. (35) is dubious for non-random systems: for example, for a Fermi liquid, the scale $\Omega \simeq 1/\tau_{\mathrm{e-e}} \sim N(0)T^2$, so that it is impossible to satisfy $T \ll \Omega$ at low T. However, in the presence of strong disorder Ω it is set by V. Since Ω is T-independent, it is possible to lower the temperature sufficiently far in the DQMC simulation to make Eq. (35) applicable.

There is a quite nice consistency between the different methodologies to characterize the phases of the model, and even the quantitative values of the conductivity. For example, Fig. 6 shows an onset of nonzero D and D_s for V in the range $3 \lesssim V \lesssim 4$ as the disorder strength is decreased. These results are based on Eqs. (30), (31). Meanwhile, the crossings of the data for ρ_{dc} in Fig. 8 indicate $V_c \sim 3.5$. Here Eq. (35) was utilized. Analysis of D based on Eq. (31) yields $V_c \sim 3.25$ and, furthermore, via Eq. (33), gives a numerical value for σ_{dc} which agrees quite closely with Eq. (35). This sort of careful cross-checking of numerics is of course essential in
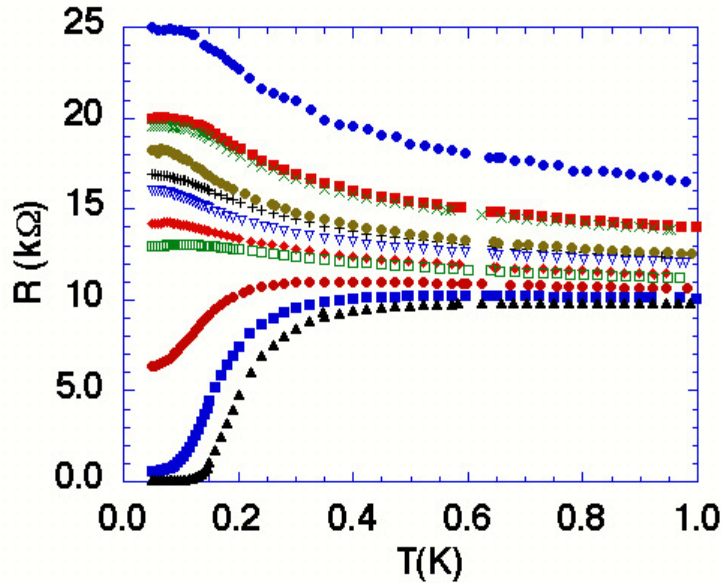
Fig. 9: *Superconducting-insulator transition in thin amorphous Bi films as a function of carrier density [17]. Note the qualitative similarity to Fig. 8. (As noted in the caption to Fig. 8, the less abrupt drop in the DQMC data is a consequence of the fact that $T > T_c$ over the temperature range shown.)*

any calculational approach, but is especially important in QMC studies of interacting fermions, where limitations of finite size and the sign problem are especially acute.

As a connection to real materials, we observe that the curves in Fig. 8 are remarkably similar to those found in the experimental literature on the two dimensional superconductor-insulator transition (SIT) in the presence of disorder [13]. In these studies, the SIT has been accessed in a wide variety of ways: by explicitly changing the degree of microscopic disorder (similar to the model studied here in which V is varied, by altering the film thickness, by applying a magnetic field, or by changing the carrier density. An example of the latter tuning method is given in Fig. 9. With DQMC, different ways of driving the SIT have also been explored with DQMC [11, 14–16].

One further method of distinguishing metals and insulators relies on the computation of the momentum-resolved spectral function $A(\mathbf{q}, \omega)$ and its sum, the density of states. The formalism is similar to that of Eq. (34), except involving the single-particle Green function $G(\mathbf{q}, \tau)$.

$$G(\mathbf{q}, \tau) = \int_{-\infty}^{+\infty} d\omega \frac{\exp(-\omega\tau)}{1 + \exp(-\beta\omega)} A(\mathbf{q}, \omega) \qquad N(\omega) = \sum_{\mathbf{q}} A(\mathbf{q}, \omega) . \qquad (36)$$

Figure 10 shows what this diagnostic discloses concerning the square lattice Hubbard Hamiltonian at half-filling. One observes that $N(\omega = 0) \to 0$ as $T \to 0$ both for weak U, the 'Slater insulator' driven by SDW order, and at intermediate U where the crossover begins to Mott insulating behavior. The size of the insulating gap is roughly given by the temperature range over which $N(\omega = 0)$ is small. This is seen to increase with increasing U.
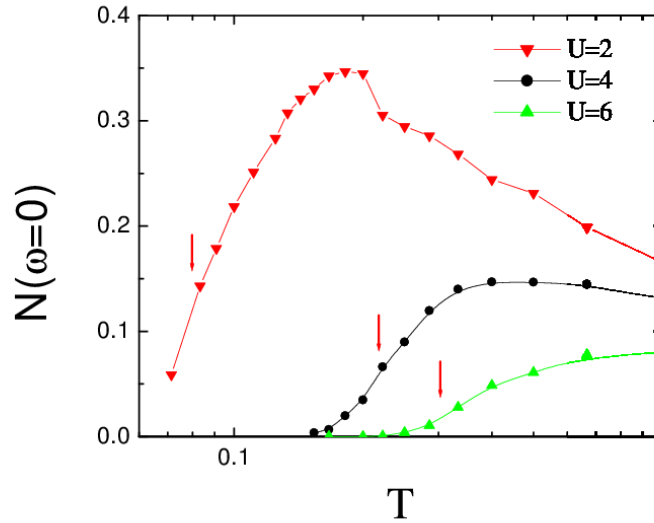
Fig. 10: *Density of states at the Fermi surface, $N(\omega = 0)$ of the half-filled Hubbard Hamiltonian as a function of temperature T for different values of the interaction strength $U = 2, 4, 6$. As $T \to 0$, the density of states vanishes in all cases. One concludes the Hubbard Hamiltonian on a square lattice with $\rho = 1$ is insulating over the entire range $0 < U < \infty$.*

8 Conclusions

We began this chapter with some simple qualitative pictures of metals and various types of insulators: (i) band insulators which arise when a TBH has several non-overlapping bands and the chemical potential lies between them; (ii) SDW and CDW insulators whose origin can be understood within a MFT treatment of interactions between the electrons or between electrons and phonons; (iii) Anderson insulators formed by disorder; and (iv) the most challenging situation, Mott insulators driven by strong interactions.

We then turned to a formal way of characterizing metals and insulators in terms of different limits of the current-current correlation function, and the implications for the conductivity and superfluid density. Our qualitative pictures of the distinction between metal and insulator in (i) and (ii) focussed on the spectrum of the Hamiltonian rather than the conductivity. The MFT treatment of the formal criteria showed the linkage between the two pictures.

The formal criteria have also been used in conjunction with QMC in the solution of the Hubbard Hamiltonian [1] to show that they indeed work when the interactions are treated more exactly than in MFT. We gave some illustrations of this approach when disorder and interactions are both present which serves as a specific model calculation for the superconducting to insulator phase transition [11], which is so well-explored experimentally [13]. Finally, we showed a few QMC results for the conductivity, spectral function, and density of states in determining insulating behavior.

It is worth noting two further approaches to the question of the metal-insulator transition which have also been widely used in QMC. The first is an analysis of the behavior of the electron self-energy at small Matsubara frequencies. For a illustration of this method, see [18]. The second is an analytic continuation of the imaginary time dependent spin, $\chi(\tau) = \langle M(\tau)M(0)\rangle$, and charge, $P(\tau) = \langle N(\tau)N(0)\rangle$, correlation functions. Here $M = \sum_i \left(n_{i\uparrow} - n_{i\downarrow}\right)$ and $N =$

$\sum_i \left(n_{i_\uparrow} + n_{i_\downarrow} \right)$. The presence of 'spin and charge gaps' in the low frequency behavior of their Laplace transforms $\chi(\omega)$ and $P(\omega)$ can be used to infer the presence of insulating behavior associated with spin and charge order. See, for example, [19].

We finish by returning to the opening of this chapter, presenting the reader with a question: In our first encounter with the idea of conductors, one associates the resistance R in Ohm's law with some sort of scattering mechanism which provides for the loss of energy. Where is such dissipation in models like the clean Hubbard Hamiltonian?

References

[1] D.J. Scalapino, S.R. White, and S. Zhang, Phys. Rev. B **47**, 7995 (1993)

[2] J.E. Hirsch, Phys. Rev. B **31**, 4403 (1985)

[3] A.A. Maradudin: *Theoretical and Experimental Aspects of the Effects of Point Defects and Disorder on the Vibrations of Crystals*, Solid State Physics **18**, 273–420 (1966)

[4] P.W. Anderson, Phys. Rev. **109**, 1492 (1958)

[5] E. Abrahams, P.W. Anderson, D.C. Licciardello, and T.V. Ramakrishnan, Phys. Rev. Lett. **42**, 673 (1979)

[6] R. Blankenbecler, D.J. Scalapino, and R.L. Sugar, Phys. Rev. D **24**, 2278 (1981)

[7] J.E. Hirsch and S. Tang, Phys. Rev. Lett. **62**, 591 (1989)

[8] C.N. Varney, C.R. Lee, Z.J. Bai, S. Chiesa, M. Jarrell, and R.T. Scalettar, Phys. Rev. B **80**, 075116 (2009)

[9] M.P.A. Fisher, P.B. Weichman, G. Grinstein, and D.S. Fisher, Phys. Rev. B **40**, 546 (1989)

[10] R.E. Peierls, Z. Phys. **80**, 763 (1933)

[11] N. Trivedi, R.T. Scalettar, and M. Randeria, Phys. Rev. B **54**, 3756 (1996)

[12] J.E. Gubernatis, M. Jarrell, R.N. Silver, and D.S. Sivia, Phys. Rev. B **44**, 6011 (1991)

[13] D.B. Haviland, Y.Liu, and A.M. Goldman, Phys. Rev. Lett. **62**, 2180, (1989);
A.F. Hebard and M.A. Paalanen, Phys. Rev. Lett. **65**, 927 (1990);
J.M. Valles, R.C. Dynes, and J.P. Garno, Phys. Rev. Lett. **69**, 3567 (1992); and
A. Yazdani and A. Kapitulnik, Phys. Rev. Lett. **74**, 3037 (1995)

[14] P.J.H. Denteneer, R.T. Scalettar, and N. Trivedi, Phys. Rev. Lett. **83**, 4610 (1999)

[15] P.J.H. Denteneer, R.T. Scalettar, and N. Trivedi, Phys. Rev. Lett. **87**, 146401 (2001)

[16] P.J.H. Denteneer and R.T. Scalettar, Phys. Rev. Lett. **90**, 246401 (2003)

[17] K.A. Parendo, K.H. Sarwa B. Tan, A. Bhattacharya, M. Eblen-Zayas, N.E. Staley, and A.M. Goldman, Phys. Rev. Lett. **94**, 197004 (2005)

[18] R.M. Noack and D.J. Scalapino, Phys. Rev. B **47**, 305 (1993)

[19] M. Vekic, J.W. Cannon, D.J. Scalapino, R.T. Scalettar, and R.L. Sugar, Phys. Rev. Lett. **74**, 2367 (1995)